JCTC Journal of Chemical Theory and Computation

Article

pubs.acs.org/JCTC

Origin of Reactivity Trends of Noble Gas Endohedral Fullerenes $Ng_2@C_{60}$ (Ng = He to Xe)

Israel Fernández,*[,†] Miquel Solà,*[,‡] and F. Matthias Bickelhaupt*[,§,∥]

[†]Departamento de Química Orgánica I, Facultad de Ciencias Químicas, Universidad Complutense, 28040 Madrid, Spain

[‡]Institut de Química Computacional i Catàlisi and Departament de Química, Universitat de Girona, Campus Montilivi, 17071 Girona, Spain

[§]Department of Theoretical Chemistry and Amsterdam Center for Multiscale Modeling (ACMM), VU University Amsterdam, De Boelelaan 1083, 1081 HV Amsterdam, The Netherlands

[∥]Institute for Molecules and Materials (IMM), Radboud University Nijmegen, Heyendaalseweg 135, NL-6525 AJ Nijmegen, The Netherlands

Supporting Information

ABSTRACT: We have computationally studied the factors governing the enhanced Diels–Alder reactivity of noble gas endohedral fullerenes $Ng_2@C_{60}$ when Ng = Ar, Kr, and Xe as compared to Ng = none, He, and Ne. To this end, we have employed the activation strain model of reactivity in combination with the energy decomposition analysis (EDA) method in DFT calculations on the Diels–Alder cycloaddition reaction between $Ng_2@C_{60}$ and 1,3-butadiene. Our results indicate that when heavier noble gas dimers are introduced inside the C_{60} cage, dramatic effects on both the geometrical and electronic structure of the fullerenic cage occur leading to a remarkable enhanced interaction between the deformed reactants along the entire reaction coordinate.

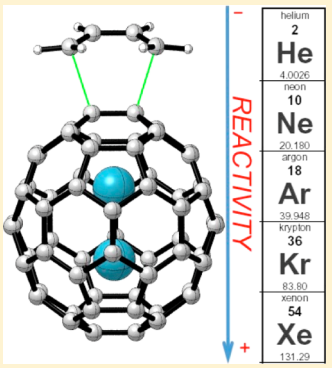

INTRODUCTION

The introduction of atoms and molecules into a fullerene cage forming the so-called endohedral fullerenes has attracted considerable interest since the discovery of the first fullerene in 1985.[1] This is mainly due to the effect of the endohedral fragment that can strongly modify the properties and reactivity of the fullerene cage. For these reasons, endohedral metallofullerenes have been (and still are) experimentally and theoretically studied because of their potential applications in diverse fields like medicine, biology, electronics, photovoltaics, and nanotechnology.[2]

An important family of endohedral fullerenes is constituted by fullerenes encapsulating noble gas (Ng) atoms in their cages. Among them, those having two Ng atoms in their structure (Ng_2@fullerene) have been particularly challenging since the theoretical prediction of their possible formation by Giblin and co-workers in 1997.[3] Only one year later, the first members of the $Ng_2@C_{70}$ family, that is, the ones with Ng = He and Ne, were experimentally identified.[4] Moreover, these experiments provided data about the possible formation of $Ne_2@C_{60}$, although the evidence found was not conclusive.[4b] Later on in 2002, Sternfeld et al. succeeded in introducing for the first time two helium atoms into C_{60}, therefore producing $He_2@C_{60}$.[5]

The bonding situation of the endohedral $Ng_2@C_{60}$ fullerenes has been studied in detail by Krapp and Frenking recently.[6] Whereas the two lightest congeners, $He_2@C_{60}$ and $Ne_2@C_{60}$, were theoretically predicted to exhibit properties that are essentially the same as those of free C_{60}, the bonding situation in the heaviest analogue $Xe_2@C_{60}$ is clearly different. Indeed, a genuine chemical bond exists between both xenon atoms in this species, a situation that resembles that found for HXeXeF and related species that also exhibit Xe–Xe bonds.[7] Therefore, a markedly different reactivity should be expected when going from helium to xenon in the $Ng_2@C_{60}$ family.

Solà and co-workers have thoroughly studied the regioselectivity of the Diels–Alder reaction between 1,3-butadiene and all nonequivalent bonds of noble gas endohedral compounds $Ng@C_{60}$ and $Ng_2@C_{60}$.[8] In agreement with the prediction by Frenking and Krapp,[6] it was found that that introduction of noble gas dimers He_2 and Ne_2 in C_{60} has almost no effect on the exohedral reactivity compared to free C_{60}.[8] As a result, the cycloaddition is clearly favored at the [6,6]- over the [5,6]-bonds in the fullerene cage for these species. Differently, the encapsulation of heavier noble gas dimers clearly enhances the reactivity of the cage, both under thermodynamic and kinetic control. As a consequence, the formation of [6,6]- and [5,6]-cycloadducts is equally viable in the case of $Xe_2@C_{60}$.

Although possible mechanisms were suggested by Solà et al.,[8] the physical factors behind the remarkable decrease in the

Received: May 22, 2014
Published: May 23, 2014

dx.doi.org/10.1021/ct500444z | J. Chem. Theory Comput. 2014, 10, 3863–3870

Diels–Alder activation barrier (from about 13 kcal/mol in the process involving $He_2@C_{60}$ to 5 kcal/mol with $Xe_2@C_{60}$) are far from being fully understood. Different to the study by Solà and co-workers,[8] herein we seek to provide a quantitative explanation to the trend in reactivity observed in the $Ng_2@C_{60}$ family of endohedral fullerenes identifying those factors that ultimately are responsible for the different computed barriers. To this end, we decided to apply the recently introduced *activation strain model* (ASM)[9] of reactivity because it has allowed us to gain quantitative insight into the factors which control how the activation barriers arise in different fundamental processes. This model, which is also known as the *distortion/interaction model*, as proposed by Houk and co-workers,[10] has successfully contributed to our current understanding of S_N2 and E2 reactions[9a,h] and different pericyclic reactions.[10,11] Interestingly, this model has been particularly useful quite recently to rationalize the exclusive formation of the [6,6]- over the [5,6]-cycloadduct in the Diels–Alder reaction between C_{60}-fullerene and cyclopentadiene.[12] Therefore, herein we will apply the ASM of reactivity to the parent [4 + 2]-Diels–Alder reaction between C_{60} and $Ng_2@C_{60}$ and 1,3-butadiene focusing on the most reactive [6,6]-bonds according to the recent report by Solà and co-workers.[8]

THEORETICAL METHODS

Computational Details. Geometry optimizations of the molecules were performed using the Gaussian09 suite of programs[13] at the dispersion-corrected M06-2X level[14] in combination with the double-ζ plus polarization def2-SVP[15] basis sets. This level has been selected because dispersion has been reported to play a crucial role in the reactivity of fullerenes.[12,16] Reactants and cycloadducts were characterized by frequency calculations and have positive definite Hessian matrices. Transition structures (TSs) show only one negative eigenvalue in their diagonalized force constant matrices, and their associated eigenvectors were confirmed to correspond to the motion along the reaction coordinate under consideration using the intrinsic reaction coordinate (IRC) method.[17]

Populations and donor–acceptor interactions have been computed using the natural bond orbital (NBO) method.[18] The energies associated with these two-electron interactions have been computed according to the following equation:

$$\Delta E^{(2)}_{\varphi\varphi^*} = -n_\varphi \frac{\langle \varphi^* | \hat{F} | \varphi \rangle^2}{\varepsilon_{\varphi^*} - \varepsilon_\varphi}$$

where $\hat{F}$ is the DFT equivalent of the Fock operator, and φ and φ^* are two filled and unfilled NBOs having ε_φ and ε_{φ^*} energies, respectively. n_φ stands for the occupation number of the filled orbital.

The program package ADF 2009.01[19] was used for the partitioning of the interaction energy by means of the EDA method (see below). Using the optimized geometries at the M06-2X/def2-SVP level, the EDA calculations were carried out at Grimme's dispersion-corrected BP86[20]-D3[21] level in conjunction with a triple-ζ-quality basis set using uncontracted Slater-type orbitals (STOs) augmented by two sets of polarization functions with a frozen-core approximation for the core electrons.[22] Auxiliary sets of s, p, d, f, and g STOs were used to fit the molecular densities and to represent the Coulomb and exchange potentials accurately in each SCF cycle.[23] Scalar relativistic effects were incorporated by applying the zeroth-order regular approximation (ZORA).[24] This level of theory, denoted BP86-D3/TZ2P//M06-2X/def2-SVP, has been selected because it provides very good results for Diels–Alder cycloaddition reactions involving C_{60}.[12]

Activation Strain Analyses of Reaction Profiles. The activation strain model is a fragment approach to understanding chemical reactions, in which the height of reaction barriers is described and understood in terms of the original reactants.[9−12] The activation strain model is a systematic extension of the fragment approach from equilibrium structures to TSs as well as *nonstationary* points, e.g., points along a reaction coordinate. Thus, the potential energy surface $\Delta E(\zeta)$ is decomposed, along the reaction coordinate ζ, into the strain $\Delta E_{strain}(\zeta)$ associated with deforming the individual reactants plus the actual interaction $\Delta E_{int}(\zeta)$ between the deformed reactants

$$\Delta E(\zeta) = \Delta E_{strain}(\zeta) + \Delta E_{int}(\zeta)$$

Here, the reaction coordinate is defined as the projection of the IRC on the forming C···C distance between the carbon atom of $Ng_2@C_{60}$ and the carbon atom of 1,3-butadiene. This reaction coordinate ζ undergoes a well-defined change in the course of the reaction from the separate reactants to the equilibrium C···C distance in the TS.

The strain $\Delta E_{strain}(\zeta)$ is determined by the rigidity of the reactants and by the extent to which groups must reorganize in a particular reaction mechanism, whereas the interaction $\Delta E_{int}(\zeta)$ between the reactants depends on their electronic structure and on how they are mutually oriented as they approach each other. It is the interplay between $\Delta E_{strain}(\zeta)$ and $\Delta E_{int}(\zeta)$ that determines if and at which point along ζ a barrier arises. The activation energy of a reaction $\Delta E^{\ddagger} = \Delta E(\zeta^{TS})$ consists of the activation strain $\Delta E^{\ddagger}_{strain} = \Delta E_{strain}(\zeta^{TS})$ plus the TS interaction $\Delta E^{\ddagger}_{int} = \Delta E_{int}(\zeta^{TS})$, thus, $\Delta E^{\ddagger} = \Delta E_{strain}{}^{\ddagger} + \Delta E_{int}{}^{\ddagger}$.

Energy Decomposition Analysis (EDA) Method. The interaction $\Delta E_{int}(\zeta)$ between the strained reactants is further analyzed in the conceptual framework provided by the Kohn–Sham molecular orbital (KS-MO) model.[25,26] Within this method, initially developed by Ziegler and Rauk[27] following a similar procedure suggested by Morokuma,[28] the interaction energy $\Delta E_{int}(\zeta)$ is further decomposed into the following physically meaningful terms

$$\Delta E_{int}(\zeta) = \Delta V_{elstat} + \Delta E_{Pauli} + \Delta E_{oi} + \Delta E_{disp}$$

The term ΔV_{elstat} corresponds to the classical electrostatic interaction between the unperturbed charge distributions of the deformed reactants and is usually attractive. The Pauli repulsion, ΔE_{Pauli}, comprises the destabilizing interactions between occupied orbitals and is responsible for any steric repulsion. The orbital interaction, ΔE_{oi}, accounts for charge transfer (interaction between occupied orbitals on one moiety with unoccupied orbitals on the other, including HOMO–LUMO interactions) and polarization (empty-occupied orbital mixing on one fragment due to the presence of another fragment). Finally, the ΔE_{disp} term takes into account the dispersion forces. Through this EDA, it has previously been possible to analyze the nature of a chemical bond in terms of electrostatic attraction versus σ-, π-, and δ-orbital (covalent) bonding.[29]

RESULTS AND DISCUSSION

Figure 1 shows the optimized structures of the TSs associated with the [4 + 2]-cycloaddition of 1,3-butadiene at the most

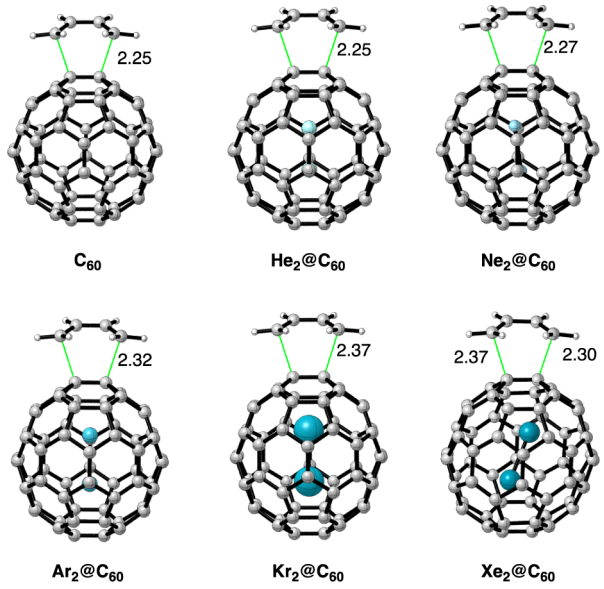

Figure 1. Optimized structures of the transition states for the [4 + 2]-cycloaddition reaction between 1,3-butadiene and $Ng_2@C_{60}$. All data have been computed at the M06-2X/def2-SVP level.

reactive [6,6]-bond of our $Ng_2@C_{60}$ molecules.[8] All processes are concerted and highly synchronous and proceed through C_s symmetric TSs with identical C···C bond distances with the notable exception of the cycloaddition involving $Xe_2@C_{60}$. In the latter process, the associated TS is clearly more asynchronous (i.e., the forming C···C distances are different) because the Xe_2 dimer is not disposed parallel to the plane of symmetry. The shortest C···C bond distance being formed corresponds to the most pyramidalized of the two attacked C atoms as confirmed by the corresponding computed hybridization ($sp^{2.16}$ vs $sp^{2.10}$). As a consequence, the reactive carbon atoms of the [6,6]-junction are differently affected by the Xe_2 fragment, which is translated into differences between the two forming C···C bond distances in the corresponding TS. Despite that, from the simple analysis of these C···C distances, it becomes clear that the lighter He_2 and Ne_2 dimers lead to TSs that strongly resemble that for C_{60}. Differently, the forming C···C bond distances are longer for Ar_2 and Kr_2 dimers thus indicating earlier TSs. Therefore, one may expect barriers and reaction energies for $He_2@C_{60}$ and $Ne_2@C_{60}$ that are similar to those of free C_{60}, while different values should be expected for the heavier $Ng_2@C_{60}$ analogues.

This prediction based on geometrical grounds is confirmed by the data in Table 1, which gathers the computed activation and reaction energies for the considered cycloaddition reactions. The energy values concur quite well with previous calculations[8] that validate the use of the M06-2X/def2-SVP method for the present study. Thus, whereas quite similar activation and reaction energies have been computed for free C_{60} and the lighter $Ng_2@C_{60}$ complexes (Ng = He, Ne), more exothermic and lower barrier processes are found for the heavier analogues. Moreover and in agreement with the Hammond–Leffer postulate,[30] there is a clear correlation between the computed activation energy $\Delta E^{\ddagger}$ and ΔE_R energy values (linear relationship with correlation coefficient of 0.99, slope of 0.27 and standard deviation of 0.35; Figure 2). As

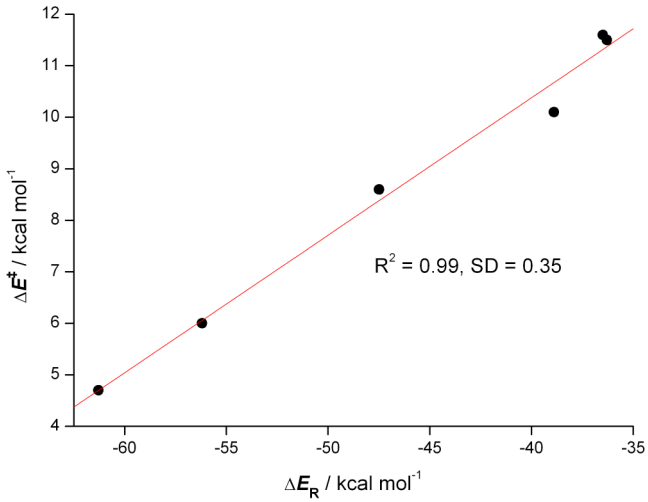

Figure 2. Plot of the reaction energies (ΔE_R) vs barrier energies ($\Delta E^{\ddagger}$) for the Diels–Alder cycloaddition reactions between $Ng_2@C_{60}$ and 1,3-butadiene.

stated by the Hammond–Leffer postulate, the larger the exothermicity is, the more reactant-like the TS is.[30] This trend agrees with the structures depicted in Figure 1. Furthermore, the computed energy values also correlate with the strain in the fullerene cage generated upon the introduction of the Ng_2 dimer. This effect can be measured by the term ΔE_{cage} (Table 1), which is the difference between the equilibrium geometry of C_{60} and the geometry adopted by the C_{60} cage in the $Ng_2@C_{60}$ species. As expected, negligible strain is introduced by the lighter noble gases He and Ne ($\Delta E_{cage} \approx 0$ kcal/mol), whereas the cage is more and more deformed when going from Ar to Xe (*vide infra*: activation strain analyses).

Table 1 also gathers the corresponding activation strain contributors to the activation energy ($\Delta E^{\ddagger} = \Delta E_{strain}{}^{\ddagger} + \Delta E_{int}{}^{\ddagger}$). Similar to the related Diels–Alder reactions between cyclo-

Table 1. Activation Strain Analysis of Diels–Alder Reactions between $Ng_2@C_{60}$ and 1,3-Butadiene[a]

entry	Ng	$\Delta E^{\ddagger}$ (E_a)	ΔE_R	$\Delta E_{int}{}^{\ddagger}$ [b]	$\Delta E_{strain}{}^{\ddagger}$ [c] (fragment $Ng_2@C_{60}$)	$\Delta E_{strain}{}^{\ddagger}$ [c] (fragment butadiene)	$\Delta E_{strain}{}^{\ddagger}$ (total)	ΔE_{cage} [d]	Ng_2 decompression [e]
1	none	11.6 (12.7)	−36.3 (−32.1)	−10.6	5.7	16.5	22.2	0.0	0.0
2	He	11.6 (13.3)	−36.5 (−31.8)	−10.2	5.5	16.3	21.8	0.1	−0.04
3	Ne	10.1 (12.4)	−38.9 (−33.6)	−9.5	3.8	15.8	19.6	0.6	−0.3
4	Ar	8.6 (9.7)	−47.5 (−43.1)	−8.6	3.8	13.4	17.2	14.5	−1.0
5	Kr	6.0 (7.5)	−56.2 (−51.2)	−8.0	2.3	11.7	14.0	30.4	−1.4
6	Xe	4.7 (6.9)	−61.3 (−56.4)	−9.1	1.0	12.8	13.8	37.4	0.03

[a]Energy in kcal/mol (in parentheses with ZPE correction) computed at M06-2X/def2-SVP. [b]$\Delta E_{int}{}^{\ddagger}$ = [E(TS)] − [E($Ng_2@C_{60}$ in geom of TS) + E(butadiene in geom of TS)]. [c]$\Delta E_{strain}{}^{\ddagger}$ = [E($Ng_2@C_{60}$ in geom of TS) + E(butadiene in geom TS)] − [E($Ng_2@C_{60}$) + E(butadiene)] . [d]ΔE_{cage} = [E(C_{60}) in geom of $Ng_2@C_{60}$] − [E(C_{60})]. [e]Ng_2 decompression = [E(Ng_2) in geom of TS] − [E(Ng_2) in geom of $Ng_2@C_{60}$].

dx.doi.org/10.1021/ct500444z | J. Chem. Theory Comput. 2014, 10, 3863−3870

pentadiene and different cycloalkenones,[31] the TS interaction between the deformed reactants $\Delta E_{int}^{\ddagger}$ remains nearly constant in the $Ng_2@C_{60}$ series (it ranges from −8.0 to −10.6 kcal/mol; Table 1). This suggests that the major contribution to the trend in activation barriers of these processes comes from the strain energy $\Delta E_{strain}^{\ddagger}$ associated with distorting the reactants from their equilibrium geometries to the geometries they adopt in the corresponding TS. Indeed, a nice linear relationship is found when plotting the computed $\Delta E^{\ddagger}$ vs $\Delta E_{strain}^{\ddagger}$, with a correlation coefficient of 0.99, slope of 1.46, and standard deviation of 0.36 (Figure 3). This correlation was obtained

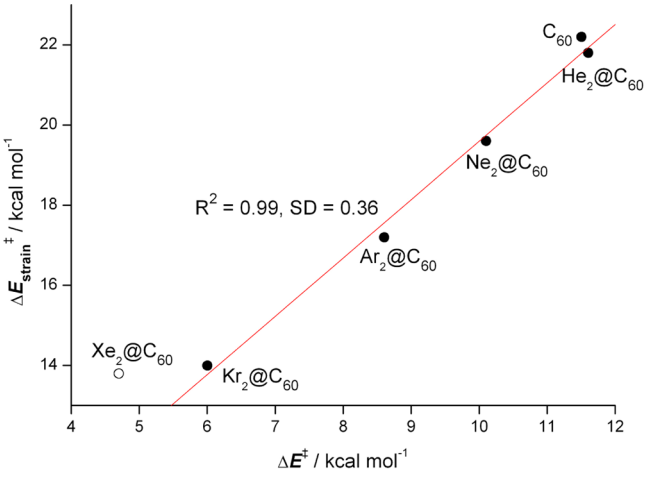

Figure 3. Plot of the activation barriers ($\Delta E^{\ddagger}$) vs activation strain energies ($\Delta E_{strain}^{\ddagger}$) for the Diels–Alder cycloaddition reactions between $Ng_2@C_{60}$ and 1,3-butadiene.

without considering the data for $Xe_2@C_{60}$, which deviates from the behavior of the entire series (see TS structures in Figure 1). When $Xe_2@C_{60}$ is also included in the analysis, the linear correlation is only slightly worse (correlation coefficient of 0.98, slope of 1.27, and standard deviation of 0.71). Finally, and resembling related [4 + 2] and [3 + 2]-cycloaddition reactions,[10,11c] the partitioning of the $\Delta E_{strain}^{\ddagger}$ into the contributions coming from the deformation of both reactants indicates that about 70–90% of the total strain energy derives from the deformation of the diene counterpart. Despite that, it is worth mentioning that there is a release of compression in the Ng_2 unit when going from the reactant to the TS (with again, the notable exception of $Xe_2@C_{60}$), which also contributes to the reduction of the activation barrier (up to −1.4 kcal/mol in $Kr_2@C_{60}$) when going down in the Ng group.

The above finding, i.e., the activation strain as the major factor controlling the cycloaddition reactions of $Ng_2@C_{60}$ species, must be interpreted with great care. This is due to the fact that the corresponding TSs occur at different locations along the reaction path (i.e., the forming C···C distances are not the same; Figure 1). Therefore, the direct comparison of the activation strain values ($\Delta E_{strain}^{\ddagger}$ and $\Delta E_{int}^{\ddagger}$) may be misleading, as shown previously in different transformations.[9i] For this reason, we decided to perform a complete activation strain analysis along the entire reaction coordinate from the separate reactants (at C···C distances of about 3.0 Å) to the corresponding TSs.

Figure 4 shows the complete activation strain diagrams (ASD) for the Diels–Alder cycloadditions along the reaction coordinate projected onto the forming C···C bond distance. All systems exhibit quite similar ASD. Thus, at the early stages of the process, the reaction profile $\Delta E(\zeta)$ monotonically becomes more and more destabilized as the reactants approach each other. As the $\Delta E_{strain}(\zeta)$ remains nearly constant at this stage, this initial increase in ΔE is ascribed to the fact that the interaction energy between the deformed reactants (ΔE_{int}), which is stabilizing at 3.0 Å particularly due to dispersion interactions, becomes more and more destabilizing as the reactants approach each other. This behavior resembles that found for other pericyclic reactions[11] and stems from the onset of overlap and Pauli repulsion between occupied π orbitals on either of the reactants. If we now further proceed along the reaction coordinate, the trend in $\Delta E_{int}(\zeta)$ inverts at a certain point (at C···C distances around 2.5 Å), after which this term becomes more and more stabilizing. The reason that the overall energy ΔE still goes up until the TS is the increase in the destabilizing strain energy, which clearly compensates the stabilization provided by $\Delta E_{int}(\zeta)$.

The differences in reactivity in the $Ng_2@C_{60}$ family are highlighted when comparing the ASD computed for $He_2@C_{60}$ and $Kr_2@C_{60}$ (Figure 4g). Thus, the $\Delta E_{strain}(\zeta)$ curve is essentially the same for both species along the reaction coordinate ζ. At variance, the $\Delta E_{int}(\zeta)$ curve is clearly more stabilizing for the heavier analogue from the very beginning of the cycloaddition reaction. As a consequence, the corresponding TS is reached earlier than when $He_2@C_{60}$ is involved in the process and has a lower activation strain ($\Delta E_{strain}^{\ddagger}$) therefore. As a result, the computed activation barrier for the heavier congeners is much lower. Therefore, it can be concluded that the stronger stabilizing interaction (and not the strain energy!) between the reactants along the entire reaction coordinate for the heavier members of the $Ng_2@C_{60}$ family is the major factor controlling the computed lower activation barriers associated with the [4 + 2]-cycloaddition reactions.

Detailed information on the different contributors to ΔE_{int} is provided by the EDA method. Figure 5 shows the EDA data along the reaction coordinate for the $Ng_2@C_{60}$ systems (Ng = He and Kr), whereas Table 2 gathers the EDA data for all species at C···C = 2.4 Å for comparison. It becomes clear that both the electrostatic attractions (measured by the ΔV_{elstat} term) and the orbital interactions (ΔE_{oi}) are the major contributors to the total interaction between the deformed reactants. Indeed, electrostatic interactions contribute to total attractions in approximately the same order of magnitude as the orbital interaction term (about 40–42%). Moreover, the contribution of dispersion is highly important at the initial stages of the process, which confirms the need to include dispersion corrections in the calculations.[12,16] However, its contribution at the proximities of the TS, although clearly not negligible, is not that significant (only about 12–15% to the total attractions).

If we now compare the EDA contributions at the same point of the reaction coordinate (Table 2), it becomes clear that the stronger interaction energy $\Delta E_{int}(\zeta)$ in the heavier noble gas-containing compounds derives mainly from a more stabilizing orbital interaction $\Delta E_{oi}(\zeta)$ between the deformed reactants. Thus, whereas the ΔV_{elstat} and ΔE_{disp} are nearly constant (about −31 kcal/mol and −11 kcal/mol, respectively), the ΔE_{oi} term is strengthened from −32 kcal/mol for Ng = He to −37 kcal/mol for Ng = Kr. Indeed, the difference in the ΔE_{oi} term ($\Delta\Delta E_{oi}$ = 5 kcal/mol) roughly matches the difference in the computed interaction energy ($\Delta\Delta E_{int}$ = 4.3 kcal/mol, when comparing He_2 and Kr_2 systems). Therefore, it can be concluded that the

dx.doi.org/10.1021/ct500444z | J. Chem. Theory Comput. 2014, 10, 3863–3870

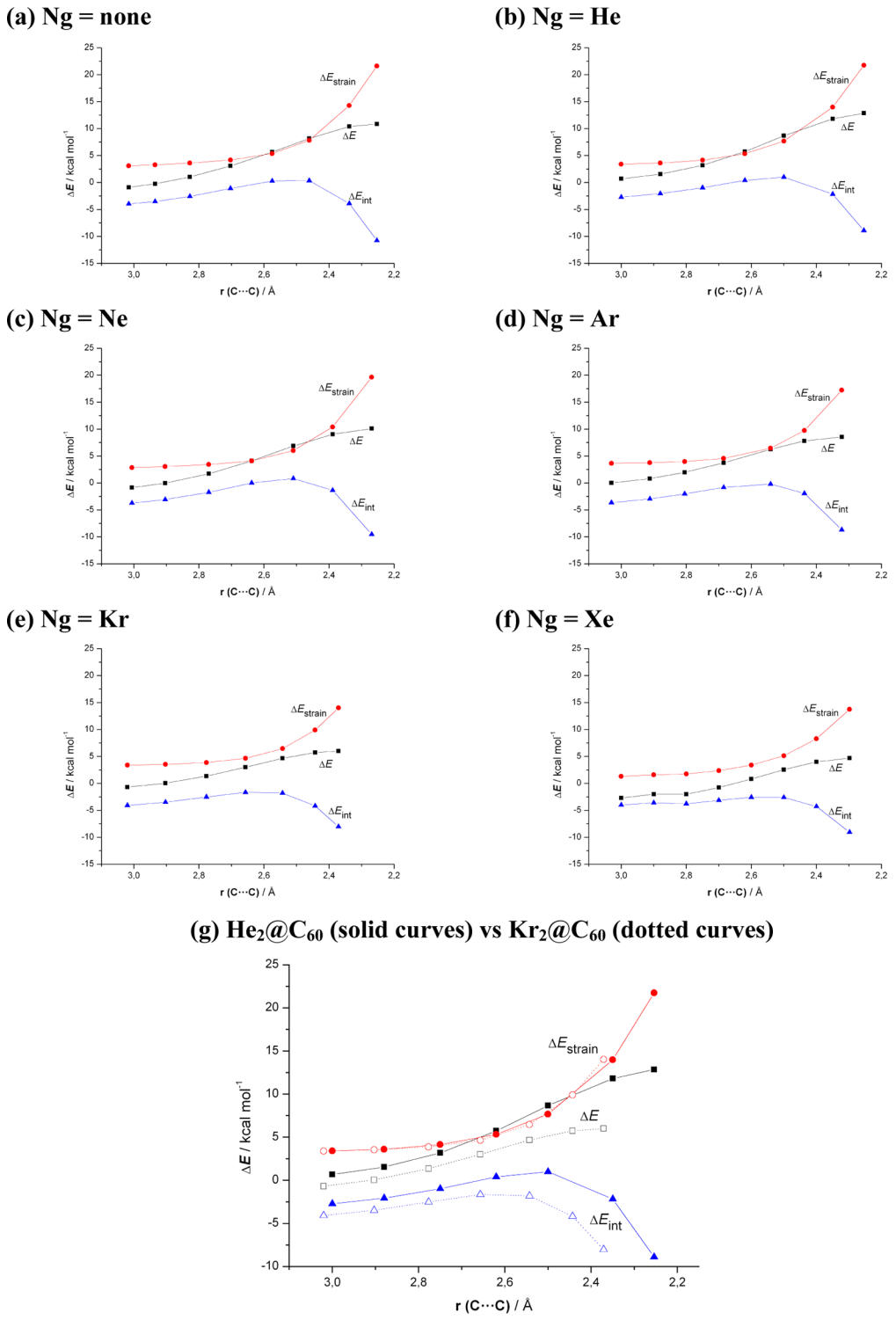

Figure 4. Activation strain diagrams of the Diels–Alder cycloaddition reaction between 1,3-butadiene and $Ng_2@C_{60}$ along the reaction coordinate projected onto the forming C···C bond distance, computed at the M06-2X/def2-SVP level.

presence of heavier noble gas dimers in the cage induces a noticeable change in the electronic structure of the cage, which enhances the interaction with the diene through stronger orbital interactions. This, in turn, is translated into a higher reactivity (i.e., lower activation barriers) for $Ng_2@C_{60}$ when Ng = Ar or Kr but not when Ng = He or Ne, which behave similarly to the free C_{60}. For the $Xe_2@C_{60}$, the general trend differs a little bit because of the large charge transfer from the noble gas dimer to the fullerene cage (vide infra).

The above conclusion is supported by the comparison of the variation in the overlap between the orbitals involved in the cycloaddition reaction, again computed for the extreme situations represented by $He_2@C_{60}$ and $Kr_2@C_{60}$ systems. Our calculations indicate that corresponding π^* molecular orbital (MO) located on the fullerene cage of the dienophile is

dx.doi.org/10.1021/ct500444z | J. Chem. Theory Comput. 2014, 10, 3863−3870

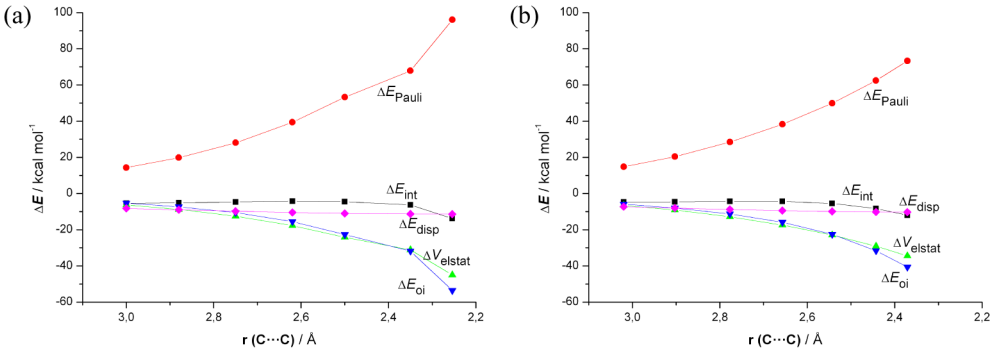

Figure 5. Energy decomposition analysis diagrams for the Diels–Alder reaction between 1,3-butadiene and $He_2@C_{60}$ (a) or $Kr_2@C_{60}$ (b).

Table 2. Energy Decomposition Analysis of Key Species in Cycloaddition between $Ng_2@C_{60}$ and 1,3-Butadiene[a]

$Ng_2@C_{60}$ + 1,3-butadiene (at C···C = 2.4 Å)						
Ng =	none	He	Ne	Ar	Kr	Xe
ΔE_{int}	−6.2	−6.2	−6.8	−8.2	−10.5	−8.9
ΔE_{Pauli}	68.0	67.9	67.9	69.0	68.5	63.4
ΔV_{elstat}[b]	−31.2 (42%)	−31.1 (42%)	−31.1 (42%)	−31.9 (41%)	−32.0 (41%)	−29.7 (41%)
ΔE_{oi}[b]	−31.7 (43%)	−31.8 (43%)	−32.4 (43%)	−34.4 (45%)	−36.8 (47%)	−32.2 (43%)
ΔE_{disp}[b]	−11.3 (15%)	−11.3 (15%)	−11.2 (15%)	−10.9 (14%)	−10.2 (13%)	−10.5 (15%)

[a]Energy values are given in kcal/mol and were computed at the BP86-D3/TZ2P+//M06-2X/def2-SVP level. [b]The percentage values in parentheses give the contribution to the total attractive interactions $\Delta V_{elstat}+\Delta E_{oi}+\Delta E_{disp}$.

more stabilized in the $Kr_2@C_{60}$ system (Figure 6a), which according to the traditional frontier molecular orbital (FMO) theory[32] should lead to a higher interaction with the π (MO) of 1,3-butadiene. Indeed, the HOMO(diene)–LUMO($Ng_2@C_{60}$) gap decreases when going from He to Xe, as was also reported by Solà and co-workers.[8] Also, the $Kr_2@C_{60}$ benefits from a somewhat better $<\pi(\text{diene})|\pi^*(Kr_2@C_{60})>$ overlap along the entire reaction coordinate (Figure 6b). For instance, at the selected C···C distance of 2.4 Å, the computed orbital overlap S = 0.087 for $Kr_2@C_{60}$, whereas a lower value of S = 0.082 was computed for $He_2@C_{60}$. Despite that, this difference in overlap along the reaction coordinate, although significant, cannot explain, let alone cause, the stronger interaction in the $Kr_2@C_{60}$ system.

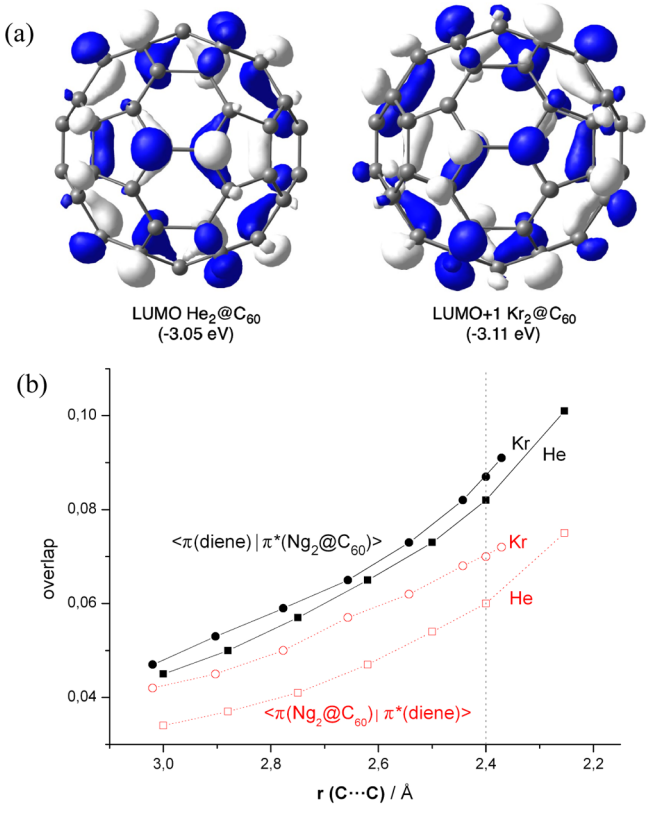

Figure 6. (a) π^* Molecular orbital of $He_2@C_{60}$ and $Kr_2@C_{60}$ (isosurface value of 0.035 au). (b) Computed $<\pi(1,3\text{-butadiene})|\pi^*(Ng_2@C_{60})>$ and $<\pi(Ng_2@C_{60})|\pi^*(1,3\text{-butadiene})>$ overlaps for the reaction between 1,3-butadiene and $Ng_2@C_{60}$ (Ng = He and Kr).

In this connection, we recall that Frenking and Krapp reported that in the case of $Xe_2@C_{60}$ there occurs a net charge transfer from the noble gas dimer to the C_{60} cage (i.e., between 1 and 2 electrons are injected into the fullerene structure, that is, $Xe_2^{q+}@C_{60}^{q-}$ with $1< q < 2$).[6] The effect of this charge transfer is a more negative potential on the C_{60} cage, which raises the energy of orbitals located on that fragment. This suggests that $Ng_2@C_{60}$ can act not only as an acceptor (i.e., as a typical dienophile) but also as a donor fragment in the cycloaddition reaction with dienes when Ng = Ar, Kr or Xe. If this hypothesis holds true, we should find a significant reverse overlap between the π MO of $Ng_2@C_{60}$ and the antibonding π^* MO of the diene. Indeed, a much higher computed reverse overlap $<\pi(Ng_2@C_{60})|\pi^*(\text{diene})>$ was found for $Kr_2@C_{60}$ compared to $He_2@C_{60}$ along the entire reaction coordinate (ranging from S = 0.042 at 3 Å to S = 0.074 at the TS distance; Figure 6b). Therefore, the combination of a higher normal electronic demand $<\pi(\text{diene})|\pi^*(Ng_2@C_{60})>$ interaction with a much stronger reverse $<\pi(Ng_2@C_{60})|\pi^*(\text{diene})>$ interaction is strongly related to the enhanced interaction with the diene when when Ng = Ar, Kr, which in turn is translated in lower activation barriers.

At this point, we were curious to analyze whether the deformed C_{60} cage already shows enhanced inverse electronic demand in its interaction with the diene because of the

dx.doi.org/10.1021/ct500444z | J. Chem. Theory Comput. 2014, 10, 3863–3870

deformation induced by the Kr_2 unit. To this end, we computed the corresponding $<\pi(C_{60})|\pi^*(\text{diene})>$ overlap at 2.4 Å using the geometry of the deformed $Kr_2@C_{60}$ system (but removing the Kr_2 dimer). Our calculations indicate a value of $S = 0.069$, which is comparable with the value of $S = 0.071$ computed for the entire $Kr_2@C_{60}$ system.

Finally, the second-order perturbation theory (SOPT) of the NBO[18] method also agrees with this description. Thus, two-electron stabilizing donations from the π(MO) located at the [6,6]-bond of $Kr_2@C_{60}$ to the π^* (MOs) of the 1,3-butadiene were found in the corresponding TS (associated SOPT energy $\Delta E^{(2)} = -6.7$ kcal/mol; Figure 7). As a result, the computed

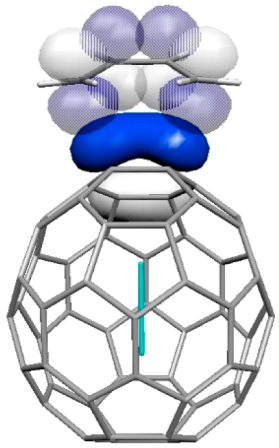

Figure 7. NBO orbitals involved in the $\pi_{[6,6]}(Kr_2@C_{60}) \rightarrow \pi^*$(butadiene) interaction in the transition state of the reaction between $Kr_2@C_{60}$ and 1,3-butadiene.

population of the π^*(MO) of butadiene is 0.22*e*, whereas a lower value of 0.17*e* was found for $He_2@C_{60}$ due to the weaker "inverse" interaction. The associated SOPT energy for this system is, however, higher ($\Delta E^{(2)} = -10.9$ kcal/mol) as a consequence of the much shorter C···C distance in the corresponding TS (Figure 1). A direct comparison at the same C···C distance (i.e., at 2.4 Å) confirms that the inverse interaction is stronger in $Kr_2@C_{60}$ ($\Delta E^{(2)} = -5.7$ kcal/mol) than in $He_2@C_{60}$ ($\Delta E^{(2)} = -4.8$ kcal/mol).

Therefore, the higher reactivity of the heavier members of $Ng_2@C_{60}$ finds its ultimate origin in the polarization induced in the cage by the Ng_2 dimer. Whereas $He_2@C_{60}$ and $Ne_2@C_{60}$ behave similarly to free C_{60}, the heavier noble gases alter significantly both the geometrical and electronic structure of the cage. These changes, in turn, provoke that in addition to an increased "normal" $<\pi(\text{diene})|\pi^*(Ng_2@C_{60})>$ interaction, the "inverse" $<\pi(Ng_2@C_{60})|\pi^*(\text{diene})>$ interaction is also remarkable. As a consequence, the orbital attraction $\Delta E_{oi}(\zeta)$ between the reactants is stronger along the entire coordinate ζ which is translated into the computed lower activation barriers.

CONCLUSIONS

From the computational study reported in this paper, the following conclusions can be drawn: (1) The introduction of noble gas dimers inside the C_{60} cage provokes dramatic effects on both the geometrical and electronic structure of the fullerenic cage in the case of heavier noble gases (Ng = Ar to Xe). (2) This leads to an enhanced reactivity, both kinetically and thermodynamically, in the Diels–Alder cycloaddition reaction with 1,3-butadiene. (3) At variance, lighter noble gas dimers (Ng = He and Ne) leads to $Ng_2@C_{60}$ endohedral fullerenes, which behave similarly to free C_{60}. (4) By means of the combined ASM–EDA methods, the origin of this differential behavior is found in the remarkable enhanced interaction between the deformed reactants along the entire reaction coordinate and not in the strain energy associated with the deformation of the C_{60} and diene fragments. (5) This can be mainly ascribed to stronger orbital interactions between the reactants along the reaction coordinate when Ng = Ar and Kr as a consequence of a higher "normal" $<\pi(\text{diene})|\pi^*(Ng_2@C_{60})>$ interaction and a much stronger "inverse" $<\pi(Ng_2@C_{60})|\pi^*$-(diene)> interaction.

ASSOCIATED CONTENT

Supporting Information

Cartesian coordinates (Å) and total energies (a.u., non-corrected zero-point vibrational energies included) of all the stationary points discussed in the text. This material is available free of charge via the Internet at http://pubs.acs.org.

AUTHOR INFORMATION

Corresponding Authors

*E-mail: israel@quim.ucm.es.
*E-mail: miquel.sola@udg.edu.
*E-mail: f.m.bickelhaupt@vu.nl.

Notes

The authors declare no competing financial interest.

ACKNOWLEDGMENTS

We are grateful for financial support from the Spanish MINECO (Grants CTQ2010-20714-C02-01, Consolider-Ingenio 2010, and CSD2007-00006 to I.F. and CTQ2011-23156/BQU to M.S.), CAM (S2009/PPQ-1634 to I.F.), Catalan DIUE (projects 2009SGR637 and XRQTC to M.S.), the FEDER fund for the grant UNGI08-4 × 10^{-003} to M.S., the National Research School Combination – Catalysis (NRSC-C), and The Netherlands Organization for Scientific Research (NWO/CW and NWO/EW). Support for the research of M.S. was received through the ICREA Academia 2009 prize of the Catalan DIUE.

REFERENCES

(1) (a) Heath, J. R.; Obrien, S. C.; Zhang, Q.; Liu, Y.; Curl, R. F.; Kroto, H. W.; Tittel, F. K.; Smalley, R. E. *J. Am. Chem. Soc.* **1985**, *107*, 7779. (b) Kroto, H. W.; Heath, J. R.; Obrien, S. C.; Curl, R. F.; Smalley, R. E. *Nature* **1985**, *318*, 162.

(2) (a) Hirsch, A.; Bettreich, M. *Fullerenes, Chemistry and Reactions*; Wiley-VCH: Weinheim, 2005. (b) Guha, S.; Nakamoto, K. *Coord. Chem. Rev.* **2005**, *249*, 1111. (c) Martín, N. *Chem. Commun.* **2006**, 2093. (d) Yamada, M.; Akasaka, T.; Nagase, S. *Acc. Chem. Res.* **2010**, *43*, 92. (e) Lu, X.; Akasaka, T.; Nagase, S. *Chem. Commun.* **2011**, *47*, 5942. (f) Osuna, S.; Swart, M.; Solà, M. *Phys. Chem. Chem. Phys.* **2011**, *13*, 3585. (g) Zhang, J.; Stevenson, S.; Dorn, H. C. *Acc. Chem. Res.* **2013**, *46*, 1548. (h) Popov, A. A.; Yang, S.; Dunsch, L. *Chem. Rev.* **2013**, *113*, 5989.

(3) Giblin, D. E.; Gross, M. L.; Saunders, M.; Jiménez-Vázquez, H. A.; Cross, R. J. *J. Am. Chem. Soc.* **1997**, *119*, 9883.

(4) (a) Khong, A.; Jiménez-Vázquez, H. A.; Saunders, M.; Cross, R. J.; Laskin, J.; Peres, T.; Lifshitz, C.; Strongin, R.; Smith, A. B. *J. Am. Chem. Soc.* **1998**, *120*, 6380. (b) Laskin, J.; Peres, T.; Lifshitz, C.; Saunders, M.; Cross, R. J.; Khong, A. *Chem. Phys. Lett.* **1998**, *285*, 7.

(5) Sternfeld, T.; Hoffman, R. E.; Saunders, M.; Cross, R. J.; Syamala, M. S.; Rabinovitz, M. *J. Am. Chem. Soc.* **2002**, *124*, 8786.

(6) Krapp, A.; Frenking, G. *Chem.—Eur. J.* **2007**, *13*, 8256.

(7) (a) Jiménez-Halla, J. O. C.; Fernández, I.; Frenking, G. *Angew. Chem., Int. Ed.* **2009**, *48*, 366. (b) Fernández, I.; Frenking, G. *Phys. Chem. Chem. Phys.* **2012**, *14*, 14869.
(8) Osuna, S.; Swart, M.; Solà, M. *Chem.—Eur. J.* **2009**, *15*, 13111.
(9) (a) Bickelhaupt, F. M. *J. Comput. Chem.* **1999**, *20*, 114. (b) Diefenbach, A.; Bickelhaupt, F. M. *J. Chem. Phys.* **2001**, *115*, 4030. (c) Diefenbach, A.; Bickelhaupt, F. M. *J. Phys. Chem. A* **2004**, *108*, 8460. (d) Diefenbach, A.; de Jong, G. T.; Bickelhaupt, F. M. *J. Chem. Theory Comput.* **2005**, *1*, 286. (e) van Stralen, J. N. P.; Bickelhaupt, F. M. *Organometallics* **2006**, *25*, 4260. (f) de Jong, G. T.; Bickelhaupt, F. M. *ChemPhysChem* **2007**, *8*, 1170. (g) de Jong, G. T.; Bickelhaupt, F. M. *J. Chem. Theory Comput.* **2007**, *3*, 514. (h) Bento, A. P.; Bickelhaupt, F. M. *J. Org. Chem.* **2008**, *73*, 7290. (i) van Zeist, W.-J.; Bickelhaupt, F. M. *Org. Biomol. Chem.* **2010**, *8*, 3118.
(10) Selected examples: (a) Ess, D. H.; Houk, K. N. *J. Am. Chem. Soc.* **2007**, *129*, 10646. (b) Ess, D. H.; Houk, K. N. *J. Am. Chem. Soc.* **2008**, *130*, 10187. (c) Ess, D. H.; Jones, G. O.; Houk, K. N. *Org. Lett.* **2008**, *10*, 1633. (d) Hayden, A. E.; Houk, K. N. *J. Am. Chem. Soc.* **2009**, *131*, 4084. (e) Liu, F.; Paton, R. S.; Kim, S.; Liang, Y.; Houk, K. N. *J. Am. Chem. Soc.* **2013**, *135*, 15642.
(11) (a) Fernández, I.; Bickelhaupt, F. M.; Cossío, F. P. *Chem.—Eur. J.* **2009**, *15*, 13022. (b) Fernández, I.; Cossío, F. P. *Curr. Org. Chem.* **2010**, *14*, 1578. (c) Fernández, I.; Cossío, F. P.; Bickelhaupt, F. M. *J. Org. Chem.* **2011**, *76*, 2310. (d) Fernández, I.; Bickelhaupt, F. M.; Cossío, F. P. *Chem.—Eur. J.* **2012**, *18*, 12395. (e) Fernández, I.; Bickelhaupt, F. M. *J. Comput. Chem.* **2012**, *33*, 509. (f) Faza, O. N.; López, C. S.; Fernández, I. *J. Org. Chem.* **2013**, *78*, 5669. (g) Fernández, I.; Bickelhaupt, F. M. *J. Comput. Chem.* **2014**, *35*, 371. (h) Fernández, I. *Phys. Chem. Chem. Phys.* **2014**, *16*, 7662. (i) Fernández, I.; Bickelhaupt, F. M.; Cossío, F. P. *Chem.—Eur. J.* **2014**, DOI: 10.1002/chem.201303874. (j) Fernández, I.; Bickelhaupt, F. M. *Chem. Soc. Rev.* **2014**, DOI: 10.1039/c4cs00055b.
(12) Fernández, I.; Solà, M.; Bickelhaupt, F. M. *Chem.—Eur. J.* **2013**, *19*, 7416.
(13) Frisch, M. J.; Trucks, G. W.; Schlegel, H. B.; Scuseria, G. E.; Robb, M. A.; Cheeseman, J. R.; Scalmani, G.; Barone, V.; Mennucci, B.; Petersson, G. A.; Nakatsuji, H.; Caricato, M.; Li, X.; Hratchian, H. P.; Izmaylov, A. F.; Bloino, J.; Zheng, G.; Sonnenberg, J. L.; Hada, M.; Ehara, M.; Toyota, K.; Fukuda, R.; Hasegawa, J.; Ishida, M.; Nakajima, T.; Honda, Y.; Kitao, O.; Nakai, H.; Vreven, T.; Montgomery, J. A., Jr.; Peralta, J. E.; Ogliaro, F.; Bearpark, M.; Heyd, J. J.; Brothers, E.; Kudin, K. N.; Staroverov, V. N.; Kobayashi, R.; Normand, J.; Raghavachari, K.; Rendell, A.; Burant, J. C.; Iyengar, S. S.; Tomasi, J.; Cossi, M.; Rega, N.; Millam, N. J.; Klene, M.; Knox, J. E.; Cross, J. B.; Bakken, V.; Adamo, C.; Jaramillo, J.; Gomperts, R.; Stratmann, R. E.; Yazyev, O.; Austin, A. J.; Cammi, R.; Pomelli, C.; Ochterski, J. W.; Martin, R. L.; Morokuma, K.; Zakrzewski, V. G.; Voth, G. A.; Salvador, P.; Dannenberg, J. J.; Dapprich, S.; Daniels, A. D.; Farkas, Ö.; Foresman, J. B.; Ortiz, J. V.; Cioslowski, J.; Fox, D. J. *Gaussian 09, Revision B.01*, Gaussian, Inc.: Wallingford, CT, 2009.
(14) Zhao, Y.; Schultz, N. E.; Truhlar, D. G. *J. Chem. Theory Comput.* **2006**, *2*, 364.
(15) Weigend, F.; Ahlrichs, R. *Phys. Chem. Chem. Phys.* **2005**, *7*, 3297.
(16) (a) Osuna, S.; Swart, M.; Solà, M. *J. Phys. Chem. A* **2011**, *115*, 3491. (b) García-Borrás, M.; Osuna, S.; Swart, M.; Luis, J. M.; Solà, M. *Chem. Commun.* **2013**, *49*, 1220. (c) García-Borràs, M.; Luis, J. M.; Swart, M.; Solà, M. *Chem.—Eur. J.* **2013**, *19*, 4468.
(17) González, C.; Schlegel, H. B. *J. Phys. Chem.* **1990**, *94*, 5523.
(18) (a) Foster, J. P.; Weinhold, F. *J. Am. Chem. Soc.* **1980**, *102*, 7211. (b) Reed, A. E.; Weinhold, F. *J. Chem. Phys.* **1985**, *83*, 1736. (c) Reed, A. E.; Weinstock, R. B.; Weinhold, F. *J. Chem. Phys.* **1985**, *83*, 735. (d) Reed, A. E.; Curtiss, L. A.; Weinhold, F. *Chem. Rev.* **1988**, *88*, 899.
(19) ADF Molecular Modeling Suite, Scientific Computing and Modeling. http://www.scm.com.
(20) (a) Becke, A. D. *Phys. Rev. A* **1988**, *38*, 3098. (b) Perdew, J. P. *Phys. Rev. B* **1986**, *33*, 8800.
(21) Grimme, S.; Antony, J.; Ehrlich, S.; Krieg, H. *J. Chem. Phys.* **2010**, *132*, 154104.
(22) Snijders, J. G.; Baerends, E. J.; Vernoojs, P. *At. Data Nucl. Data Tables* **1981**, *26*, 483.
(23) Krijn, J.; Baerends, E. J. *Fit Functions in the HFS-Method*; Internal Report (in Dutch); Vrije Universiteit Amsterdam, The Netherlands, 1984.
(24) (a) van Lenthe, E.; Baerends, E. J.; Snijders, J. G. *J. Chem. Phys.* **1993**, *99*, 4597. (b) van Lenthe, E.; Baerends, E. J.; Snijders, J. G. *J. Chem. Phys.* **1994**, *101*, 9783. (c) van Lenthe, E.; Ehlers, A.; Baerends, E. J. *J. Chem. Phys.* **1999**, *110*, 8943.
(25) (a) Bickelhaupt, F. M.; Baerends, E. J. In *Reviews in Computational Chemistry*; Lipkowitz, K. B., Boyd, D. B., Eds.; Wiley-VCH: New York, 2000; Vol. *15*, p 1. (b) Lein, M.; Frenking, G. In *Theory and Applications of Computational Chemistry: The First 40 Years*; Dykstra, C. E., Frenking, G., Kim, K. S., Scuseria, G. E., Eds.; Elsevier: Amsterdam, 2005; p 291.
(26) von Hopffgarten, M.; Frenking, G. *WIREs Comput. Mol. Sci.* **2012**, *2*, 43.
(27) Ziegler, T.; Rauk, A. *Theor. Chim. Acta* **1977**, *46*, 1.
(28) Morokuma, K. *J. Chem. Phys.* **1971**, *55*, 1236.
(29) Selected examples: (a) Frenking, G.; Wichmann, K.; Fröhlich, N.; Loschen, C.; Lein, M.; Frunzke, J.; Rayón, V. M. *Coord. Chem. Rev.* **2003**, *238*−*239*, 55. (b) Fernández, I.; Frenking, G. *Chem.—Eur. J.* **2006**, *12*, 3617. (c) Fernández, I.; Frenking, G. *Chem. Commun.* **2006**, 5030. (d) Krapp, A.; Bickelhaupt, F. M.; Frenking, G. *Chem.—Eur. J.* **2006**, *12*, 9196. (e) Fernández, I.; Frenking, G. *Faraday Discuss.* **2007**, *135*, 403. (f) Fernández, I.; Frenking, G. *Chem.—Eur. J.* **2007**, *13*, 5873. (g) Pierrefixe, S. C. A. H.; Bickelhaupt, F. M. *Chem.—Eur. J.* **2007**, *13*, 6321. (h) Cadenbach, T.; Bollermann, T.; Gemel, C.; Fernández, I.; von Hopffgarten, M.; Frenking, G.; Fischer, R. A. *Angew. Chem. Int. Ed.* **2008**, *47*, 9150. (i) Fernández, I.; Frenking, G.; Uggerud, E. *Chem.—Eur. J.* **2009**, *15*, 2166. (j) Fernández, I.; Duvall, M.; Wu, J. I.-C.; Schleyer, P. v. R.; Frenking, G. *Chem.—Eur. J.* **2011**, *17*, 2215. (k) Cases, M.; Frenking, G.; Duran, M.; Solà, M. *Organometallics* **2002**, *21*, 4182. (l) Bickelhaupt, F. M.; Solà, M.; Fonseca-Guerra, C. *J. Chem. Theory Comput.* **2006**, *2*, 965.
(30) (a) Hammond, G. S. *J. Am. Chem. Soc.* **1955**, *77*, 334. (b) Pross, A. *Theoretical and Physical Principles in Organic Reactivity*; Wiley: New York, 1995.
(31) Paton, R. S.; Kim, S.; Ross, A. G.; Danishefsky, S. J.; Houk, K. N. *Angew. Chem., Int. Ed.* **2011**, *50*, 10366.
(32) (a) Fleming, I. *Frontier Orbitals and Organic Chemical Reactions*. Wiley, New York, 1976. See also: (b) Ess, D. H.; Jones, G. O.; Houk, K. N. *Adv. Synth. Catal.* **2006**, *348*, 2337 and references therein..